

A Minor Axis Surface Brightness Profile for M31¹

Mike J. Irwin¹, Annette M. N. Ferguson², Rodrigo A. Ibata³, Geraint F. Lewis⁴, Nial R. Tanvir⁵

ABSTRACT

We use data from the Isaac Newton Telescope *Wide Field Camera* survey of M31 to determine the surface brightness profile of M31 along the south-east minor axis. We combine surface photometry and faint red giant branch star counts to trace the profile from the innermost regions out to a projected radius of 4° (≈ 55 kpc) where $\mu_V \sim 32$ mag arcsec⁻²; this is the first time the M31 minor axis profile has been mapped over such a large radial distance using a single dataset. We confirm the finding by Pritchet & van den Bergh (1994) that the minor axis profile can be described by a single de Vaucouleurs law out to a projected radius of 1.4 degrees or ≈ 20 kpc. Beyond this, the surface brightness profile flattens considerably and is consistent with either a power-law of index ~ -2.3 or an exponential of scalelength 14 kpc. The fraction of the total M31 luminosity contained in this component is $\approx 2.5\%$. While it is tempting to associate this outer component with a true Population II halo in M31, we find that the mean colour of the stellar population remains approximately constant at $V-i \approx 1.6$ from $0.5 - 3.5^\circ$ along the minor axis. This result suggests that the same metal-rich stellar population dominates both structural components.

Subject headings: galaxies: individual (M31)– galaxies: evolution – galaxies: halos – Local Group – galaxies: stellar content – galaxies: structure

¹Based on observations made with the Isaac Newton Telescope operated on the Island of La Palma by the Isaac Newton Group in the Spanish Observatorio del Roque de los Muchachos of the Instituto de Astrofísica de Canarias

¹Institute of Astronomy, Madingley Road, Cambridge UK CB3 0HA; mike@ast.cam.ac.uk

²Institute for Astronomy, University of Edinburgh, Blackford Hill, Edinburgh UK EH9 3HJ

³Observatoire de Strasbourg, 11, rue de l'Université, F-67000, Strasbourg, France

⁴Institute of Astronomy, School of Physics, A29, University of Sydney, NSW 2006, Australia

⁵Centre for Astrophysics Research, University of Hertfordshire, College Lane, Hatfield UK AL10 9AB

1. Introduction

The structure of galaxies at very large galactocentric radii (and hence very faint light levels) is a subject of much current interest. From a theoretical perspective, high resolution simulations of galaxy formation indicate that many signatures of the galaxy assembly process should lie buried in these parts (e.g. Bullock, Kravtsov, & Weinberg (2001); Bullock & Johnston (2004)). The discovery of stellar substructure in galaxy halos (e.g. Majewski et al. (2003); Ibata et al. (2001); Ferguson et al. (2002); Shang et al. (1998)) lends strong support to the idea that galaxies assemble, at least in part, via the accretion of small satellite systems. However, equally important constraints on galaxy formation come from studies of their smooth stellar components with key questions concerning the profile, shape and composition of stellar halos and outer disks. Unfortunately, the low surface brightness of these parts (typically $\mu \gtrsim 28 - 29$ mag arcsec⁻²) poses a significant challenge for studies of diffuse unresolved light and few robust constraints have been derived to date from this technique (e.g. Dalcanton & Bernstein (2002); Morrison et al. (1994)).

Several recent studies have mapped galaxy structure to well below the usual depths of traditional surface photometry by taking advantage of unique datasets and/or innovative analysis techniques. Zibetti et al. (2004) carefully rescale and stack over 1000 edge-on galaxies selected from the Sloan Digital Sky Survey (SDSS) in order to detect emission as faint as $\mu_r \sim 31$ mag arcsec⁻². They find evidence for the presence of flattened red power-law ($c/a \sim 0.6, \rho \propto r^{-3}$) stellar halos around disk galaxies. Zibetti & Ferguson (2004) take advantage of the unprecedented depth of the Hubble Ultra Deep Field to study faint extra-planar emission around an edge-on galaxy at $z = 0.32$ and find a similar power-law halo component dominating at very faint surface brightness levels. On the other hand, deep star count analyses of the low luminosity systems NGC 300 and M33 indicate the presence of only a disk component at very large radii (Bland-Hawthorn et al. (2005), Ferguson et al. in prep).

In this Letter, we exploit the Issac Newton Telescope *Wide-Field Camera* survey of M31 to determine the surface brightness profile of the galaxy along the minor axis. Using the combination of traditional surface photometry in highly-crowded regions and faint red giant branch (RGB) star counts in diffuse regions, we are able to trace the profile from the innermost regions of M31 out to a projected radius of 4° or ≈ 55 kpc. The contiguous nature of the survey provides excellent sampling of the profile at all radii and the ability to distinguish local density enhancements in M31 from fluctuations in background galaxy counts and the foreground distribution of Galactic stars. Previous results from our photometric survey have been reported in Ibata et al. (2001) and Ferguson et al. (2002).

2. Observations

The Isaac Newton Telescope *Wide Field Camera* is a 4-chip EEV 4k×2k CCD mosaic camera which images ≈ 0.29 square degrees. During the period Sept 2000–Jan 2004, we used this camera to image 163 contiguous fields (corresponding to ≈ 40 square degrees) in the disk and halo of M31. Our map covers an elliptical region of semi-major (minor) axis $4(2.5)^\circ$ or $\approx 55(34)$ kpc, with an additional ~ 10 square degree extension towards the south.

Images were taken in the Johnson V and Gunn *i* bands under mainly good atmospheric conditions and typical seeing better than $1.2''$. The exposure time of 800-1000s per passband per field allowed us to reach $i = 23.5$, $V = 24.5$ ($S/N \approx 5$) which is sufficient to detect individual red giant branch (RGB) stars to $M_V \approx 0$ and main sequence stars to $M_V \approx -1$ at the distance of M31. Details of the survey observing strategy and pipeline reductions are discussed in Ibata et al. (2001) and Ferguson et al. (2002).

Objects are classified as noise artifacts, galaxies, or stars according to their morphological structure on all the images. In the outer halo fields, we typically detect equal numbers of resolved and unresolved sources within the magnitude and color ranges of interest. Of the extended sources, approximately 20% are ‘compact’ in the sense of being within the 3-5 sigma range of the stellar boundary in the classification statistic and having an ellipticity of < 0.4 . Making the plausible assumption that half of these are genuinely extended, we expect that the contamination due to mis-classified barely resolved field galaxies is small and, in general, considerably less than 10% of the total number of detected sources.

Stellar contamination from the Galactic foreground steadily increases to the north, due to the proximity of the Galactic Plane, rising smoothly from an average contamination of ≈ 13000 stars per square degree at the southern extremity of the survey to ≈ 20000 stars per square degree at the northern extremity (integrated over all magnitudes). This foreground variation, coupled with our current lack of suitable comparison fields uncontaminated by M31, is the primary uncertainty in our star counts at very large radii.

3. Constructing the Minor Axis Profile

Figure 1 shows the surface density of stellar-like sources with magnitudes and colours consistent with being RGB stars at the distance of M31. White patches in the map are either areas contaminated by saturated stars (and the nuclear region of M31) or are due to small gaps in the survey coverage. As reported in earlier papers (Ibata et al. 2001; Ferguson et al. 2002; Lewis et al. 2004), the INT WFC survey has revealed a wealth of stellar substructure in the outskirts of M31. Our focus here, however, is the smooth structure of the galaxy’s

outskirts.

The sources shown in Figure 1 are selected to have $21 < i < 22$ and $i > 26.85 - 2.85(V - i)$ and we refer to these as red RGB stars. We select blue RGB stars as stellar sources with $20.5 < i < 22.5$ and $24.85 - 2.85(V - i) < i < 26.85 - 2.85(V - i)$. The lower magnitude limits for both red and blue RGB stars are conservatively set at roughly one magnitude brighter than the survey $5\text{-}\sigma$ detection threshold to mitigate against the effects of varying completeness. If age is constant across the survey area, the red and blue selection criteria isolate metal-rich and metal-poor giants respectively.

Our large-area contiguous survey of M31 enables us to trace the surface brightness profile along the southern minor axis from the inner regions out to well beyond previously-published measurements (Pritchett & van den Bergh 1994; Durrell et al. 2004). The presence of significant substructure in the outskirts of M31, especially in the southern half of the galaxy, means the region over which to compute a representative profile must be chosen carefully. Inspection of the distribution of RGB stars orthogonal to the minor axis indicates that a region of $\pm 0.5^\circ$ on either side of the minor axis (defined as position angle of 141.9°) is free of obvious contaminating debris (see Figure 1). Debris from the giant stellar stream is a serious problem beyond $\approx 0.5^\circ$ to the west of the minor axis, whereas the north-east shelf overdensity is a problem further eastward.

In order to study the light profile in the inner regions of M31, we create a large mosaiced image from individual V- and i -band pointings resampled at $1''$ resolution. Overlaps between pointings are used to adjust for sky brightness variations during the observations. We then carry out surface photometry on this mosaic. The V- and i -band surface brightness is computed as the median value in a series of equally-spaced ($10''$) wedge-shaped bins with width increasing linearly from $100''$ in the innermost regions to $820''$ at a radius of 1° , to ensure overlap with the star counts. This sampling was chosen as a compromise between maximising resolution in the inner parts and signal-to-noise considerations in the outer parts, and minimising the number of bright star halos affecting the surface brightness photometry. This technique works well out to a radius of $\approx 0.5^\circ$ beyond which uncertainties in the overall sky level correction start to become significant. Beyond 1.0° , the sky background dominates the signal and these regions are used to determine the appropriate background value to subtract from the measured surface brightness profile.

To explore the profile further out, we employ RGB star counts computed in rectangular bins of size $3' \times 1^\circ$ (see the dashed lines in Figure 1). The validity of using this technique in conjunction with the direct surface brightness measures rests on the fact that a significant fraction of the light of an old stellar population originates in luminous RGB stars. The RGB star counts are split into blue and red RGB components and are used to extend the V- and

i-band profiles respectively. We correct the star counts for incompleteness due to crowding using the prescription of Irwin & Trimble (1984), although by restricting the use of star counts to the outer regions of M31 the correction is never larger than a factor of two. An additional additive correction to the star counts is made for “background” contamination arising from foreground Milky Way stars and unresolved background galaxies. This level is set by computing the surface density of unresolved sources with magnitudes and colours typical of M31 RGB stars in several of the outermost pointings in our INT WFC survey, lying at radii 4–5°. We assume that these sources are entirely contaminants and while this may not be strictly correct due to a possibly very extended M31 halo (Guhathakurta et al. 2005), it does not have a major impact on the profile over the surface brightness range that we are considering here.

Finally, the star count profiles are shifted vertically to overlap with the photometrically-calibrated inner surface brightness profiles in the radial range 0.4–0.7°. In joining the profiles in this way, we implicitly assume that the slope of the luminosity function is constant with radius; that is, that the RGB star counts represent a constant fraction of the total flux at each position. This assumption seems valid given the lack of an obvious radial metallicity gradient within the M31 halo (Ferguson et al. (2002); Durrell et al. (2004), and see Section 4). Figure 2 shows the combined V- and *i*-band minor axis profiles. That the profiles are smooth across the overlap region serves as reassurance that no features or slope changes are introduced as a result of combining profiles constructed from the different techniques.

4. Results and Discussion

Overlaid on the surface brightness profile in Figure 2 is the de Vaucouleurs $R^{1/4}$ law that Pritchet & van den Bergh (1994) found best-characterised their minor axis profile over the radial range 1" to 1.5°. This model has an effective radius of $r_e = 0.1^\circ$ or 1.4 kpc, derived from scaling Pritchet & van den Bergh (1994)’s original value to the currently-accepted distance of 785 kpc (McConnachie et al. 2005; Durrell, Harris, & Pritchet 2001). As can be seen, this model also provides an excellent description of the profile derived here. The slight mismatch between the data and the model at radii of 0.1–0.4° occurs where the contribution of the disk component – which we have neglected here – to the minor axis profile is a maximum (Walterbos & Kennicutt 1988; Pritchet & van den Bergh 1994).

This result goes beyond merely confirming the findings of previous studies. Earlier work has relied on measurements from various sources in order to cover a sufficient radial range along the minor axis (Pritchet & van den Bergh 1994). These measurements have not only been made by different authors with different telescopes/instruments, but often in different

filters, and several assumptions have been required to place them on a common photometric system. The uncertainty this has introduced into the minor axis profiles published to date has been unclear. Our ability to determine the profile from 0.02 to 4° using a single dataset thus represents a significant advance.

Beyond a radius of 1.4° , the minor axis profile levels off relative to the extrapolation of the inner $R^{1/4}$ law. Such a flattening has also recently been reported by Guhathakurta et al. (2005) but at a slightly larger radius of 2.2° . These authors refer to this outer component as the ‘halo’. Overlaid on the left-hand panel of Figure 2 is a projected NFW profile (Navarro et al. 1997; Yang et al. 2003) of scale-radius 0.25° or 3.4 kpc. NFW profiles provide excellent descriptions of the density profiles of dark matter halos and asymptote towards $\rho \propto r^{-3}$ at large radii (though we note that an NFW dark matter halo would have a much larger scale length than the above). Figure 2 shows that while an NFW profile with this scale radius provides a reasonably good match to the outer parts of the minor axis profile, the radial density fall-off is actually somewhat steeper than r^{-3} . Indeed, a power-law fit to the minor axis surface brightness profile beyond 1.5° yields an index of ≈ -2.3 . Alternatively, the outer profile can also be adequately fit with an exponential of scalelength 1° or ~ 14 kpc.

An advantage of NFW and exponential profiles is that they remain finite when integrated from the centre (although in the case of an NFW profile an outer radius limit is also required, which we adopt here as 100 kpc). Using the parameters noted previously, we find that the absolute V-band magnitude of the halo is -17.1 and -17.0 for an NFW and exponential profile respectively. Allowing for 0.2 mag of extinction and a total M31 V-band magnitude of $M_{V_0} = -21.1$ (Hodge 1994), this implies the fraction of the total M31 luminosity contained in the halo component is only $\approx 2.5\%$.

Figure 3 shows a V-*i* minor axis colour profile constructed from the individual V- and *i*-band surface brightness profiles. The colour reddens over the inner 0.5° but then levels off to a constant value of ≈ 1.6 , within the extent of the uncertainties. Rather remarkably, the break in the minor axis profile at 1.4° is unaccompanied by any obvious change in colour, implying that the same metal-rich stellar population dominates at all radii. This is further supported by Durrell et al. (2004)’s finding of the same metallicity distribution function at 20 and 30 kpc, radii which bridge the region where the surface brightness profile changes slope. Taken together, these results make it difficult to associate the flat outer component seen along the minor axis of M31 with a classical ‘Population II’ halo.

Understanding the nature of this new structural component in M31 will require further photometric and spectroscopic studies of its constituent populations. For example, do these stars exhibit a distinct kinematical signature from the rotating inner components (Ibata et al. 2005)? Does the halo shape remain constant with increasing radius? Pritchett & van

den Bergh (1994) find no evidence for the halo becoming significantly rounder out to $\sim 2^\circ$ however inspection of Figure 1 indicates that the off-axis fields they used to measure the flattening would have been contaminated by stellar debris.

Our finding of a red power-law halo component at large radius in M31 is especially interesting in light of the Zibetti et al. (2004) and Zibetti & Ferguson (2004) analyses of faint extraplanar emission around distant galaxies. The stellar halos observed in those studies fall off as $\rho \propto r^{-3}$ to r^{-4} , similar to the $\rho \propto r^{-3.3}$ found here. These indices also compare favourably to that of the Milky Way halo (Preston, Schectman, & Beers 1991; Kinman, Suntzeff, & Kraft 1994; Ivezić et al. 2000). Additional studies of the faint outskirts of galaxies will be required to understand whether these power-law components are indeed ubiquitous and to derive constraints on their origin.

REFERENCES

- Bellazzini, M., Cacciari, C., Federici, L., Fusi Pecci, F., & Rich, M. 2003, *A&A*, 405, 867
- Bland-Hawthorn, J., Vlahić, M., Freeman, K., & Draine, B. 2005, ArXiv Astrophysics e-prints, astro-ph/0503488
- Brown, T. M., Ferguson, H. C., Smith, E., Kimble, R. A., Sweigart, A. V., Renzini, A., Rich, R. M., & VandenBerg, D. A. 2003, *ApJ*, 592, L17
- Bullock, J. S., Kravtsov, A. V., & Weinberg, D. H. 2001, *ApJ*, 548, 33.
- Bullock, J. S. & Johnston, K. V. 2004, in proceedings of *Satellites and Tidal Streams*, eds . F. Prada, D. Martinez-Delgado, T. Mahoney, in press (astro-ph/0401625)
- Dalcanton, J. J., & Bernstein, R. A. 2002, *AJ*, 124, 1328
- Durrell, P. R., Harris, W. E., & Pritchett, C. J. 2001, *AJ*, 121, 2557
- Durrell, P. R., Harris, W. E., & Pritchett, C. J. 2004, *AJ*, 128, 260
- Ferguson, A. M. N., Irwin, M. J., Ibata, R. A., Lewis, G. F. & Tanvir, N. R. 2002, *AJ*, 124, 1452
- Ferguson, A. M. N., Johnson, R. A., Faria, D. C., Irwin, M. J., Ibata, R. A., Johnston, K. V., Lewis, G. F., & Tanvir, N. R. 2005, *ApJ*, 622, L109

- Guhathakurta, P., Ostheimer, J. C., Gilbert, K. M., Rich, R. M., Majewski, S. R., Kalirai, J. S., Reitzel, D. B., & Patterson, R. J. 2005, ArXiv Astrophysics e-prints, astro-ph/0502366
- Hodge, P., in 5th Canary Islands Winter School of Astrophysics, Edited by C. Munoz-Turon and F. Sanchez. Cambridge University Press, 1994., p.1
- Holland, S., Fahlman, G. G., & Richer, H. B. 1996, AJ, 112, 1035
- Holland, S. 1998, AJ, 115, 1916
- Ibata, R., Irwin, M., Lewis, G., Ferguson, A. M. N., & Tanvir, N. 2001b, Nature, 412, 49
- Ibata, R., Chapman, S., Ferguson, A. M. N., Lewis, G., Irwin, M., & Tanvir, N. 2005, ArXiv Astrophysics e-prints, astro-ph/0504164
- Irwin, M. & Lewis, J. 2001, New Astronomy Review, 45, 105
- Ivezic, Z. et al., 2000, AJ, 120, 963
- Kinman, T. D., Suntzeff, N. B., & Kraft, R. P. 1994, AJ, 108, 1722
- Klypin, A., Zhao, H., & Somerville, R. S. 2002, ApJ, 573, 597
- Johnston, K. V., Hernquist, L., & Bolte, M. 1996, ApJ, 465, 278
- Lewis, G. F., Ibata, R. A., Chapman, S. C., Ferguson, A. M. N., McConnachie, A. W., Irwin, M. J., & Tanvir, N. 2004, PASA, 21, 203
- Majewski, S. R., Skrutskie, M. F., Weinberg, M. D., & Ostheimer, J. C. 2003, ApJ, 599, 1082
- McConnachie, A. W., Irwin, M. J., Ferguson, A. M. N., Ibata, R. A., Lewis, G. F., & Tanvir, N. 2005, MNRAS, 356, 979
- Morrison, H. L., Boroson, T. A., & Harding, P. 1994, AJ, 108, 1191
- Mould, J. & Kristian, J. 1986, ApJ, 305, 591
- Navarro, J. F., Frenk, C. S., & White, S. D. M. 1997, ApJ, 490, 493
- Preston, G. W., Schectman, S. A. & Beers, T. C. 1991, ApJ, 375, 121
- Pritchett, C. J., & van den Bergh, S. 1994, AJ, 107, 1730

- Reitzel, D. B., Guhathakurta, P., & Gould, A. 1998, *AJ*, 116, 707
- Reitzel, D. B., & Guhathakurta, P. 2002, *AJ*, 124, 234
- Schlegel, D. J., Finkbeiner, D. P., & Davis, M. 1998, *ApJ*, 500, 525
- Shang, Z., et al. 1998, *ApJ*, 504, L23
- Walterbos, R. A. M. & Kennicutt, R. C. 1988, *A&A*, 198, 61
- Yang, X. H., Mo, H. J., Kauffmann, G., & Chu, Y. Q. 2003, *MNRAS*, 339, 387
- Zibetti, S., White, S. D. M., & Brinkmann, J. 2004, *MNRAS*, 347, 556
- Zibetti, S., & Ferguson, A. M. N. 2004, *MNRAS*, 352, L6

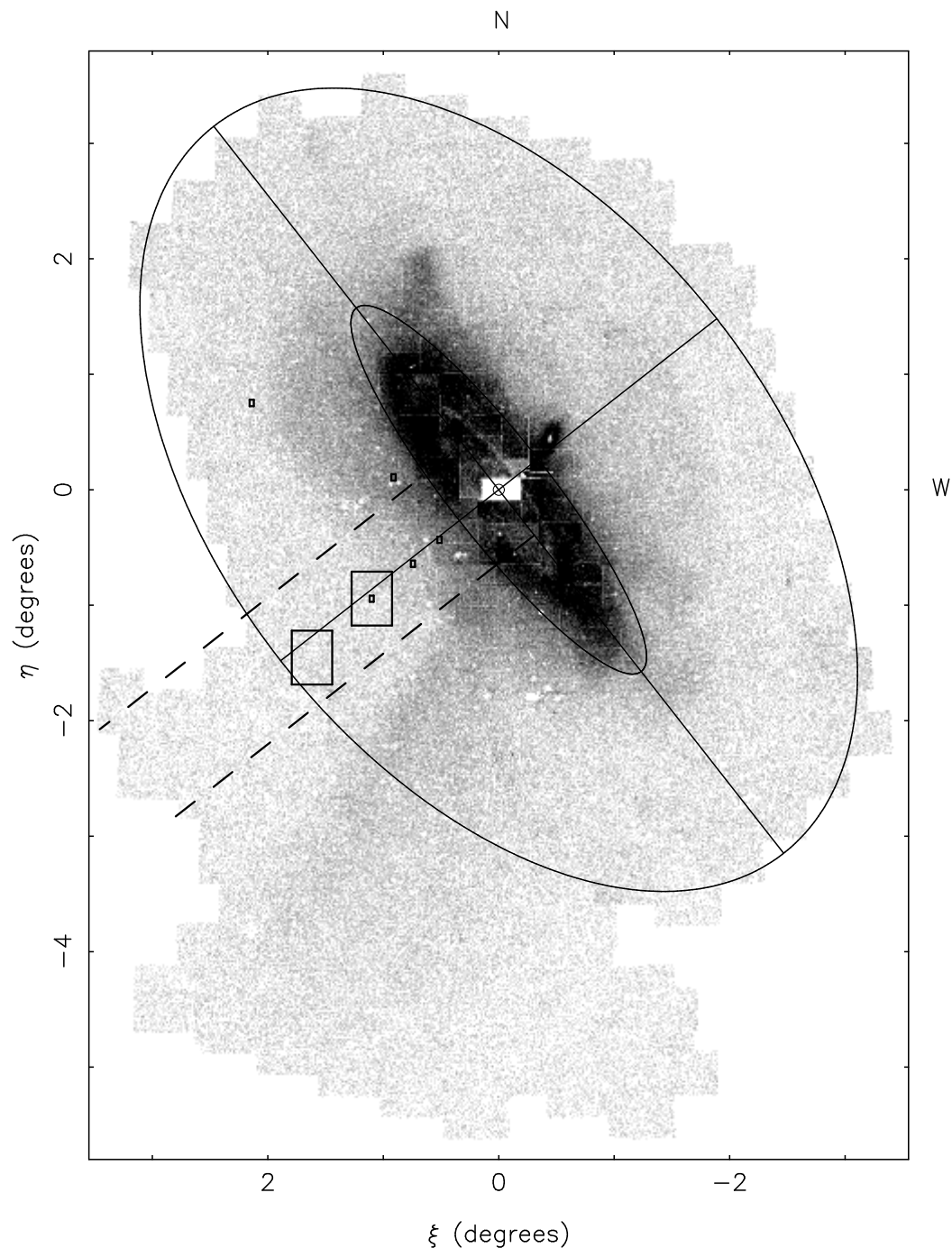


Fig. 1.— A standard coordinate projection of the surface density of red RGB stars in a 40 square degree area around M31. The outer ellipse denotes a flattened ellipsoid (aspect ratio 3:5) of semi-major axis 55 kpc, while the inner ellipse has a semi-major axis 27 kpc and represents the approximate extent of the bright disk. The area used to compute the minor axis surface brightness profile ($\pm 0.5^\circ$ of the minor axis) is delineated by the dashed lines. Overlaid are the locations of the fields observed by Durrell, Harris, & Pritchett (2001) and Durrell et al. (2004) (large rectangles) and Pritchett & van den Bergh (1994) (small rectangles).

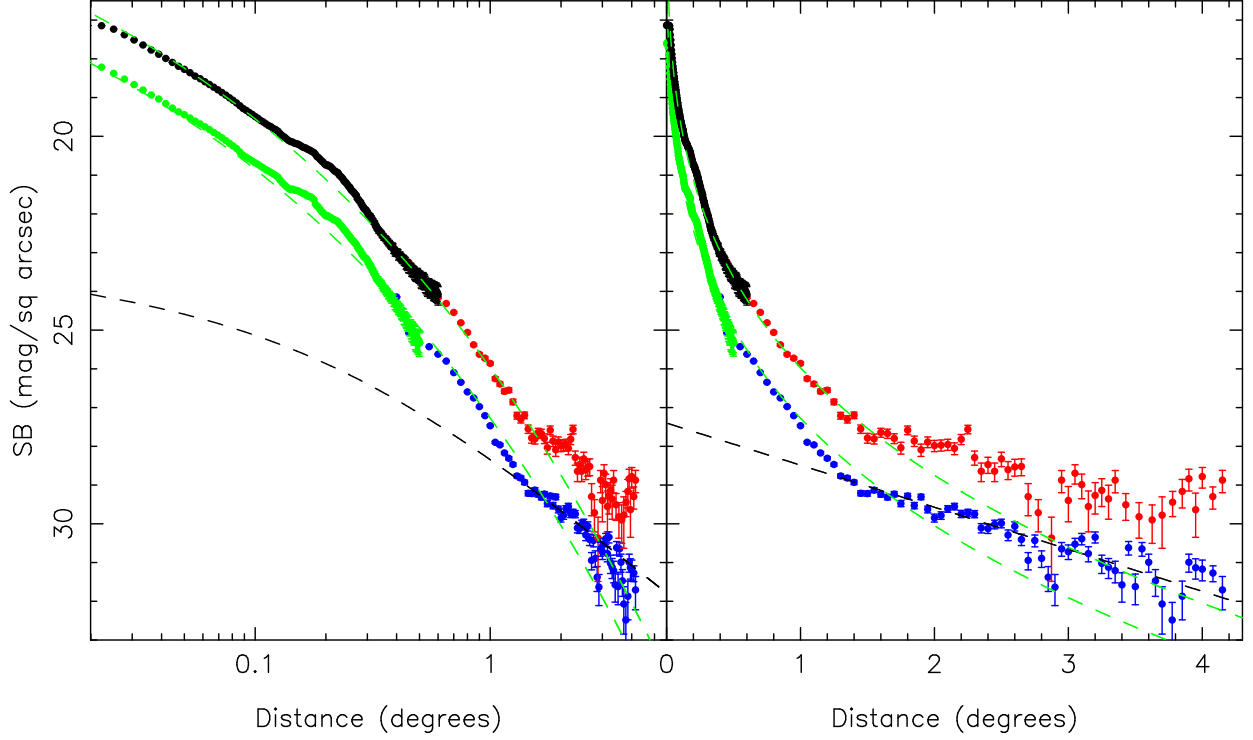


Fig. 2.— The effective V and *i*-band minor axis profiles shown on a log-log (left) and log-linear (right) scale. The V-band profile is illustrated in green and blue and the *i*-band profile in black and red. The green and black circles are derived from surface photometry whereas the blue and red points are derived from star counts in the magnitude and colour selection boxes described in the text. The error bars reflect a combination of poissonian and background uncertainties. The green dashed lines show a de Vaucouleurs $R^{1/4}$ law with $b_{eff} = 1.4$ kpc. The dashed black line in the left-hand panel shows an NFW profile computed with scale-radius=3.4 kpc and, in the right-hand panel, an exponential profile computed with scalelength=13.7 kpc.

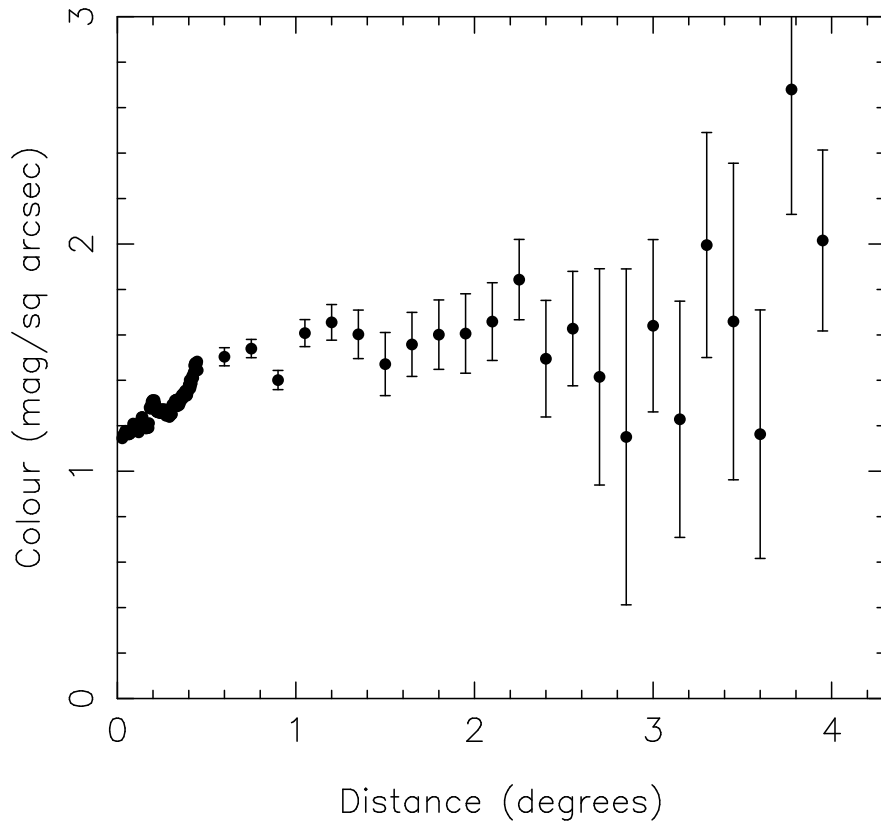


Fig. 3.— A minor axis colour profile constructed from the effective V and i -band profiles in Figure 2. The star count data are binned up into 0.2° bins; error bars reflect uncertainties in the individual profiles as well as the dispersion within bins.